A Simple yet Effective Metric for Assessing Doppler Tolerance

Jennifer E. Quirk, *IEEE Grad Student Member*, Rachel J. Chang, *IEEE Grad Student Member*, Jonathan W. Owen, *IEEE Grad Student Member*, Shannon D. Blunt, *IEEE Fellow*, Patrick M. McCormick, *IEEE Member*

***Abstract*--The Doppler tolerance of a waveform refers to its behavior when subjected to fast-time Doppler shift imposed by scattering that involves nonnegligible radial velocity. The delay/Doppler ambiguity function characterizes this behavior, with notable attributes of Doppler-dependent mismatch loss (relative to zero Doppler) and possible offset in delay estimation. Previous effort has gone into establishing decision-based criteria where a binary judgement of being Doppler tolerant or not is made.**

Here, we consider the utility of a simple, yet effective measure of the *degree* of Doppler tolerance arising from a fundamental attribute of the ambiguity function that is also convenient to extract. This metric is examined in the context of a variety of different waveform classes including traditional linear/nonlinear chirps, noise-like signals, and phase codes. Extension to wideband operation is likewise considered. The purpose in doing so is to establish a consistent standard that can be readily applied, thereby permitting easy assessment across different parameterizations, as well as introducing a Doppler "quasi-tolerant" trade-space that can ultimately inform automated/cognitive waveform design in increasingly complex and dynamic radio frequency (RF) environments.

I. Introduction

A Doppler tolerant waveform is one that is approximately invariant – from a scattering signal-to-noise ratio (SNR) perspective – in the presence of appreciable radial velocity between the platform and scatterer, thereby directly impacting the radar receiver's ability to maintain accurate detection and localization. Understanding of Doppler tolerance is achieved through evaluation of the well-known delay/Doppler ambiguity function [1-5], which is formed by correlating the transmitted waveform (having zero Doppler shift) with reflected versions thereof over a span of anticipated Doppler frequency shifts and possibly temporal dilation or contraction (if wideband). These frequency/temporal changes to the reflected waveform introduce a mismatch loss as a function of Doppler, the assessment of which generally dictates whether a given waveform is deemed Doppler tolerant or not.

When waveform bandwidth is sufficiently narrowband [6,7] temporal distortion is conveniently negligible, resulting in Woodward's ambiguity function [1]. Alternatively, the wideband ambiguity function is a general model that accounts for both Doppler frequency and temporal changes [2-5]. The degree of loss resulting from Doppler is also dependent on the radar waveform, where more complex signal structures tend to be associated with less Doppler tolerance.

A variety of criteria have been posed to decide whether or not a given waveform is Doppler tolerant. A general definition in the wideband context is given in [5], where a waveform is categorized as Doppler tolerant if the delay/Doppler ridge (presumed present) across some Doppler span is nearly equal to the value at zero Doppler. In [8], a Doppler tolerance definition is posed based on an approximation of the maximum target velocity at which the linear frequency modulation (LFM) waveform incurs 3 dB of mismatch loss. A similar fixed-loss perspective is taken in [9] specific to orthogonal frequency-division multiplexing (OFDM) signals, albeit with respect to the expected loss since this signal is random. For such random signals, this X-dB loss approach is effectively just evaluating the mainlobe in Doppler, which is actually waveform-invariant in the constant amplitude case. A formal definition relying on set theory is proposed in [10], where tolerance depends on the Doppler span within which the ambiguity function meets a chosen threshold, with this formal definition recently being applied to Costas and Sudoku codes [11].

A common theme across these approaches is the setting of some manner of threshold to demarcate Doppler tolerance or not. While doing so is certainly useful, the growing complexity of the radio frequency (RF) environment and the drive toward increasingly dynamic and multifunction radar operation also suggests the need for a measurable *degree* of Doppler tolerance that relaxes the binary decision condition and can be readily factored into the growing design trade-space for waveforms that are likewise becoming more complex.

This work was supported by the Office of Naval Research under Contract #N00014-20-C-1006. DISTRIBUTION STATEMENT A. Approved for Public Release.

J.E. Quirk is with the Radar Systems & Remote Sensing Lab (RSL) and the Electrical Engineering & Computer Science (EECS) Department, University of Kansas, Lawrence, KS 66045 USA (email: jennifer_quirk@ku.edu).

R.J. Chang is with RSL/EECS, University of Kansas (email: rjchang@ku.edu).

J.W. Owen is with RSL/EECS, University of Kansas (email: j842o274@ku.edu).

S.D. Blunt is with RSL/EECS, University of Kansas, (email: sdblunt@ittc.ku.edu).

P.M. McCormick is with RSL/EECS, University of Kansas (email: pmccormick@ku.edu).

A useful Doppler tolerance metric also needs to be broadly applicable since a growing litany of possible radar signals may be employed depending on the particular objective [12]. The well-known LFM waveform is widely regarded as Doppler tolerant [2,5] since its matched filter response exhibits sufficiently low loss as a function of Doppler, albeit with an attendant offset in the range estimate. A subclass of nonlinear FM (NLFM) waveforms known as hyperbolic FM (HFM) exhibits wideband Doppler tolerance [13,14] and has recently been experimentally demonstrated to detect high-speed projectiles (bullets) [15]. When hunting for food [16] bats have also been observed to emit HFM waveforms in the acoustic regime, where sensitivity to Doppler is far greater.

In passive radar, examination of the ambiguity function is needed for transmitter source selection [17-19] and rapid evaluation may be necessary in some cases [20]. Extension of ambiguity function analysis to multiple-input multiple output (MIMO) systems is also of recent interest [21-23].

Waveforms such as orthogonal frequency division multiplexing (OFDM) [9], amplitude modulated (AM) noise [24,25], and phase/frequency coded waveforms [26-28] are widely considered to be Doppler intolerant – or more precisely, Doppler *selective* – and exhibit a near-thumbtack ambiguity function response. Such signals may be beneficial for precise range/Doppler estimation at the cost of requiring a bank of Doppler-tuned matched filters to address mismatch loss. Random FM (RFM) waveforms [29-31] and more recent spectrally-shaped versions thereof [32], possess noise-like characteristics within an FM structure amenable to high power transmission, and have likewise been shown to exhibit a near-thumbtack ambiguity function [33]. Certain forms of hybrid radar/ communication waveforms (e.g. [34-36]) even combine attributes of both Doppler tolerant and selective structures, further complicating the distinction. As recently noted in [37]:

> *"True waveform diversity necessarily requires that we be able to use waveforms that may be Doppler intolerant. This is exacerbated by the fact that radars are migrating to higher and higher frequencies; in addition, emerging threats call for detecting and tracking very high-speed targets such as hypersonic weapons that travel at speeds exceeding Mach 5."*

Consequently, establishing a convenient and effective way to measure the degree of Doppler tolerance should prove useful from a waveform design/selection standpoint, particularly in increasingly complex and stressing environments.

Recently, as part of the development of a gradient-based FM waveform optimization approach [38], it became useful to pose a simple measure of Doppler tolerance to facilitate comparison between the resulting waveforms. Here we generalize that metric to a form compatible with other waveform design objectives that provides a loss measure of a waveform's degree of Doppler tolerance. We then examine the metric's behavior for a variety of waveform classes, which in turn leads to broad inferences about the Doppler "quasi-tolerant" trade-space.

II. Doppler Tolerance Metric

For a given waveform $s(t)$, the narrowband (magnitude-squared) ambiguity function characterizes the matched filter response as a function of relative delay τ and Doppler shift f_D via

$$A(\tau, f_D) = \left| \int_{-\infty}^{\infty} e^{j2\pi f_D t} s(t)\, s^*(t+\tau)\, dt \right|^2 . \qquad (1)$$

Doppler tolerance as an attribute is then conceptually understood [5] to indicate $A(\tau, f_D) \approx A(0,0)$ for meaningful values of f_D in the given context. The most well-known example is the LFM chirp, which exhibits a prominent delay-Doppler ridge that decreases gradually as a function of Doppler. Because the presence (or absence) of this ridge is the prevailing factor that determines Doppler tolerance (or not), it stands to reason that capturing some measurable aspect of it that can be distilled into a single value would be useful. Of course, this approach does raise the question: what is appropriate to measure when no clear ridge is present?

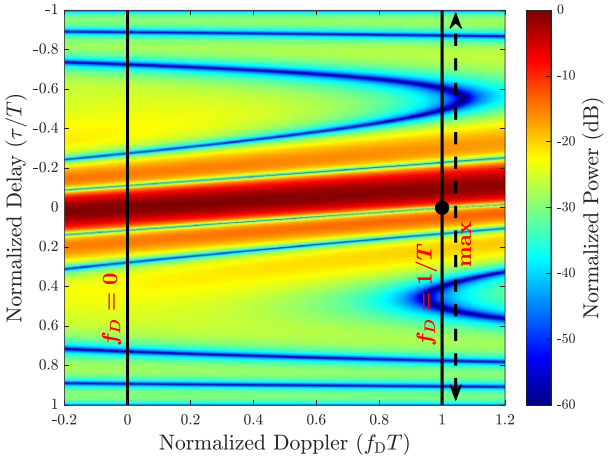

Fig. 1. LFM ambiguity function for $TB = 10$ indicating $f_D = 0$ (left black line) and $f_D = +1/T$ (right black line), where the first Doppler null occurs at the black dot, and with the maximum value determined across delay over the $f_D = +1/T$ line to capture the ridge (if it exists).

In [38] this question was answered by selecting a reference point on the ambiguity function that is common to any constant amplitude waveform (a typical requirement to maximize power efficiency). Specifically, for such waveforms the zero-delay cut of (1) across Doppler is a sinc^2 function regardless of the particular waveform. The chosen reference point [38] is then at the first Doppler null of this zero-delay cut, which occurs at $\pm 1/T$ for T the pulse width, since the response at that location is zero (the black dot in Fig. 1). The maximum value of (1) across delay τ is then determined for this

particular Doppler, with $A(\tau=0, f_D=\pm 1/T)=0$ ensuring that said maximum is not due to the sinc^2 function, thereby enabling capture of the ridge (if it exists).

If a delay/Doppler ridge does *not* exist for a given waveform, then the largest delay/Doppler sidelobe along this $f_D=\pm 1/T$ cut is obtained, which may very well be far from the mainlobe in range. For any practical values of time-bandwidth (*TB*) product this sidelobe would be considerably lower than the peak at $A(0,0)$, thus indicating poor Doppler tolerance.

As a function of f_D we can attempt to capture the delay/Doppler ridge (if it exists) by first determining

$$\eta(f_D)=\frac{\max_{\tau} A(\tau, f_D)}{A(0,0)}, \tag{2}$$

which is useful to define for the waveform assessments to follow. The metric from [38] is then realized via

$$\psi = 10\log_{10}\left(\eta(f_D=1/T)\right) \text{ dB}. \tag{3}$$

We can subsequently approximate the Doppler loss roll-off as a line (in dB per unit Doppler) that runs between ($f_D = 0$, loss = 0 dB) and ($f_D = \pm 1/T$, loss = ψ dB) via

$$\begin{aligned}\text{loss}(f_D) &\approx \frac{(\psi-0)}{(1/T-0)}\left|f_D\right| \text{ dB} \\ &= \psi T\left|f_D\right| \text{ dB},\end{aligned} \tag{4}$$

as depicted for various different waveforms in the next section. Thus $\pm\psi T$ (for positive/negative f_D) represents the slope for this *loss line approximation*, with ψ being the waveform-dependent portion.

While determining the maximum response over τ at the reference point $f_D = 1/T$ does allow (3) to avoid the sinc^2 response (by evaluating at $A(\tau=0, f_D=\pm 1/T)=0$, or $-\infty$ dB), it can also be instructive to perform a similar assessment at different points along the interval $(0, 1/T]$ in Doppler. Consequently, we can generalize (3) as

$$\psi_\alpha = 10\log_{10}\left(\eta(f_D=\alpha/T)\right) \text{ dB} \tag{5}$$

for $\alpha\in(0,1]$, where deviation from collinearity across the ensuing line approximations provides further insight into measuring Doppler tolerance. Moreover, one could easily consider the values realized by (5), or their associated loss line approximations, in comparison to the zero-delay sinc^2 Doppler mainlobe roll-off as another means to characterize tolerance since the latter would clearly dominate for a thumbtack ambiguity function.

It is also sometimes the case that an amplitude taper is applied to some form of chirped waveform on transmit (to be match filtered on receive) or on receive-only (as a mismatched filter), with the latter being more common due to transmitter considerations. Because the taper is known, its impact on the zero-delay cut across Doppler (i.e. deviation from sinc^2) is likewise known and can be readily accounted for when determining the first null location. Doing so simply entails replacing T with $\tilde{T}$ in (3)-(5), where $\tilde{T}=T/\beta$ and $\beta\geq 1$. For instance, rectangular, Hamming, and 30-dB Taylor windows involve setting β = 1, 2, or 1.509, respectively.

Accounting for (5) and tapering generalizes the loss line approximation of (4) to

$$\begin{aligned}\text{loss}(f_D) &\approx \frac{(\psi_\alpha-0)}{(\alpha\beta/T-0)}\left|f_D\right| \text{ dB} \\ &= \left(\frac{\psi_\alpha T}{\alpha\beta}\right)\left|f_D\right| \text{ dB}.\end{aligned} \tag{6}$$

Now the overall slope is $\pm\psi_\alpha T/(\alpha\beta)$, with ψ_α/β comprising the waveform+taper dependent portion. Consequently, we can use this notion of line-approximated slope to compare the degree of Doppler tolerance for all manner of constant amplitude and tapered waveforms, including forms in which tapering is performed only on receive (mismatched filtering).

Finally, note that waveforms with non-deterministic amplitude envelopes, such as random noise or orthogonal frequency division multiplexing (OFDM), do not adhere to a sinc^2 structure for their entire zero-delay Doppler cut, which instead is variable outside the Doppler mainlobe. However, taking the expectation of (1) for these random signals still yields a first Doppler null at $\pm 1/T$ [9,25], and thus (2)-(6) remain applicable.

III. Doppler Tolerance Analysis of Waveforms

The following examines the application of the simple Doppler tolerance metric from Sect. II for a variety of different waveform classes, including linear/nonlinear chirps, noise-like signals, and phase codes. Since these various signals have different spectral shapes, there are myriad ways in which consistent bandwidth *B* could be imposed. Here we select *B* to be 3-dB bandwidth because it is convenient to establish for all the waveform classes. Unless the impact of time-bandwidth product (*TB*) is being specifically varied, it is set to *TB* = 100 in all cases.

A. Linear/Nonlinear Chirps

We first consider a comparison between LFM, which for narrowband operation represents the benchmark for Doppler tolerance, and three different NLFM waveforms; namely LFM/tan-FM [39], tansec-FM [40], and tan-FM [41]. Fig. 2 illustrates the delay-Doppler ridge projected onto the Doppler axis (obtained via (2)) for each of these chirped waveforms (solid traces) and associated loss line approximations (dashed traces) via (3) and (4). The sinc^2 zero-delay response (black trace) is also depicted, with the gray vertical line denoting where the metric is assessed. Noting symmetry, only positive Doppler is shown.

The LFM ridge is almost identical to its loss line approximation (indistinguishable blue traces), while the others deviate more quickly beyond $f_D T$ = 1 (gray line). Depending on the Doppler span one expects for a given application, these NLFM waveforms may be considered marginally tolerant, with the LFM/tan-FM case (red traces) being noticeably more tolerant than the others (yellow and purple traces). Moreover, while all of them appear to exceed the sinc^2 response, the line

approximations (using (3) and (4)) for these latter two waveforms cut through the sinc^2 mainlobe for f_DT less than roughly 0.25, another indication of poorer tolerance.

Viewed another way, the loss lines for the latter two waveforms (yellow/purple) fall below their respective ridges for $f_DT > 1$, while the LFM/tan-FM (red) loss line trends above its ridge. Such behavior illustrates the inherent slope deflection across the ridge itself, which could be a way to classify quasi-tolerant waveforms.

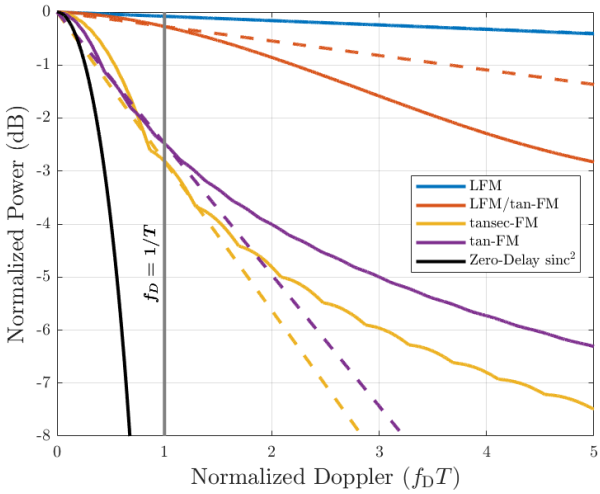

Fig. 2. Delay/Doppler ridge η (solid traces) via (2) and loss line approximation (dashed traces) via (3) and (4) for LFM and NLFM chirps at $TB = 100$. The black trace is the zero-delay sinc^2 response and the gray line denotes where $f_D = 1/T$ is evaluated.

It is also useful to examine the loss progression via (5) for these waveforms, along with the associated sinc^2 roll-off. Specifically, for α set to 0.25, 0.50, and 1.0, Table I lists the resulting ψ_α values, where we observe that LFM clearly exhibits the most gradual loss progression (as expected) and appears to follow a linear trend (in dB). The LFM/tan-FM loss is only 1.5× greater than LFM at $\alpha = 0.25$, but grows to ~2.2× and ~3.4× at 0.5 then 1.0 (i.e. not a linear trend). The tansec-FM and tan-FM waveforms exhibit even greater loss, in a manner that is even more nonlinear.

TABLE I
COMPARISON OF LOSS ψ_α FROM (5) AT DIFFERENT α VALUES FOR LFM AND NLFM WAVEFORMS AT $TB = 100$

	ψ_α, $\alpha = 0.25$	ψ_α, $\alpha = 0.5$	ψ_α, $\alpha = 1.0$
LFM	–0.02004 dB	–0.04019 dB	–0.08084 dB
LFM/tan-FM	–0.03022 dB	–0.08765 dB	–0.2733 dB
tansec-FM	–0.2157 dB	–0.8686 dB	–2.815 dB
tan-FM	–0.3773 dB	–1.26 dB	–2.479 dB

If we alternatively pose Table I in terms of the slope values (ψ_α/α) as shown in Table II, we observe that LFM indeed realizes a nearly linear progression since the slope is almost invariant. The nonlinear slope trend for the other waveforms is now evident, though the nature of the nonlinearity clearly takes different forms (e.g. gradually changing slope for LFM/tan-FM and tansec-FM, vs. more abrupt then flattening slope for tan-FM).

TABLE II
COMPARISON OF APPROXIMATED LINE SLOPE (ψ_α/α) AT DIFFERENT α VALUES FOR LFM AND NLFM WAVEFORMS AT $TB = 100$

	ψ_α/α, $\alpha = 0.25$	ψ_α/α, $\alpha = 0.5$	ψ_α/α, $\alpha = 1.0$
LFM	–0.08014 dB	–0.08038 dB	–0.08084 dB
LFM/tan-FM	–0.1209 dB	–0.1753 dB	–0.2733 dB
tansec-FM	–0.8626 dB	–1.737 dB	–2.815 dB
tan-FM	–1.509 dB	–2.52 dB	–2.479 dB

As a comparison using the fixed-loss approach in [8,9], we can determine the maximum Doppler shift that achieves 1 dB loss, which can be obtained by inspection of Fig. 2. From this definition, LFM still exhibits the best Doppler tolerance, realizing a normalized Doppler shift of $f_DT = 11.75$. The remaining LFM/tan-FM, tansec-FM, and tan-FM cases result in $f_DT = 2.205$, 0.539, and 0.413, respectively. Unsurprisingly, these results qualitatively agree with the trend in Table II based on the simple metric of (5) but require a more complex assessment since they involve a two-dimensional search of the ambiguity function, which would also complicate subsequent utility for waveform design.

Another perspective is obtained by evaluating ψ from (3) as a function of TB, which is shown in Fig. 3. The poor Doppler tolerance of LFM for small TB is clearly consistent with the observation in [10]. Indeed, below TB of 3 (for tansec-FM and tan-FM) or 10 (for LFM/tan-FM) LFM actually has worse Doppler tolerance. Of course, such low values are rarely used and for $TB > 10$ we observe that LFM clearly has superior tolerance as expected, asymptotically approaching 0 dB of loss as TB increases. While LFM/tan-FM exhibits a similar behavior, asymptotically approaching –0.24 dB, the tansec-FM and tan-FM waveforms are revealed to provide ψ values that are nearly invariant to TB, albeit at a level around –2.5 to –3 dB.

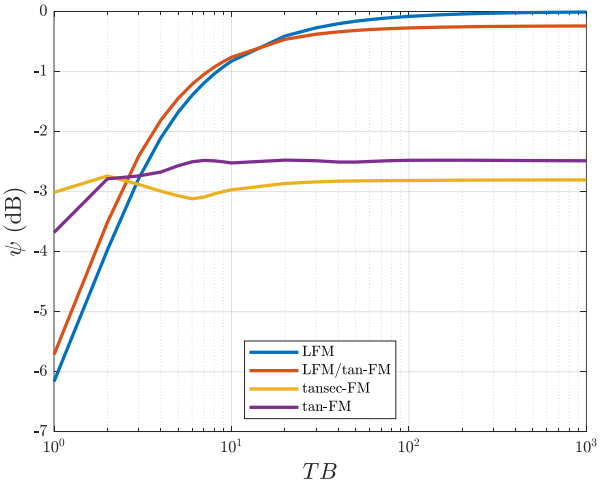

Fig. 3. Comparison of ψ from (3) for LFM and select NLFM waveforms as a function of TB from 1 to 1000.

B. *Noise-Like Waveforms*

Noise-like waveforms possess random phase and/or amplitude characteristics. The most common version in literature is simply complex noise (at baseband) [24,25]. Recent consideration has also been given to OFDM, which is widely employed in communications and involves complex symbols modulated onto a set of equally-spaced subcarriers [9]. To contend with the rigors of the high-power amplifier in most radar transmitters, RFM has also been explored [29-33], including recent efforts that perform spectral shaping to achieve better per-pulse range sidelobe performance (see [32] and references therein).

In the Doppler tolerance context, we examine each of these three types (complex noise, OFDM, spectrally shaped RFM), with the latter taking the particular form of pseudo-random optimized (PRO) FM [42] since it is representative and convenient to generate. To this mix we add the phase-attached radar/communication (PARC) waveform [35] that exemplifies the hybridization of a Doppler tolerant chirp with a Doppler selective random signal (e.g. [34-36]), thus permitting control of the quasi-tolerant trade-space.

To evaluate the Doppler-dependent loss metric in aggregate across the set of random waveforms $s_\ell(t)$ for $\ell = 1, \cdots, L$, we first determine the "average maxima" via

$$\bar{\eta}(f_{\rm D}) = \frac{1}{L}\sum_{\ell=1}^{L} \eta_\ell(f_{\rm D}), \tag{7}$$

where $\eta_\ell(f_{\rm D})$ is determined for each $s_\ell(t)$ via (2). Doing so captures either the ridge (if one exists) or the maximum sidelobe value (across delay) for each Doppler. An averaged version of the generalized metric of (5) is thus

$$\bar{\psi}_\alpha = 10\log_{10}\left(\bar{\eta}(f_{\rm D} = \alpha/T)\right) \text{ dB}, \tag{8}$$

with associated loss line approximation

$$\text{loss}(f_{\rm D}) \approx \left(\frac{\bar{\psi}_\alpha T}{\alpha}\right)|f_{\rm D}| \text{ dB}. \tag{9}$$

Here $\beta = 1$ since time-domain tapering may not be appropriate for such waveforms.

Fig. 4 depicts (2) and the ensuing loss line approximation for single instantations of each random waveform class, while Fig. 5 shows the average via (8) and (9) for $L = 1000$ independent waveforms of each class. The near-thumbtack ambiguity functions for these waveforms clearly realize Doppler selectivity, with the small variations in Fig. 4 leading to almost identical results when averaging is performed (Fig. 5). Also note that the previous X-dB fixed loss assessment of [8,9] is essentially waveform-independent for these cases since doing so only captures the Doppler mainlobe for any reasonable loss value.

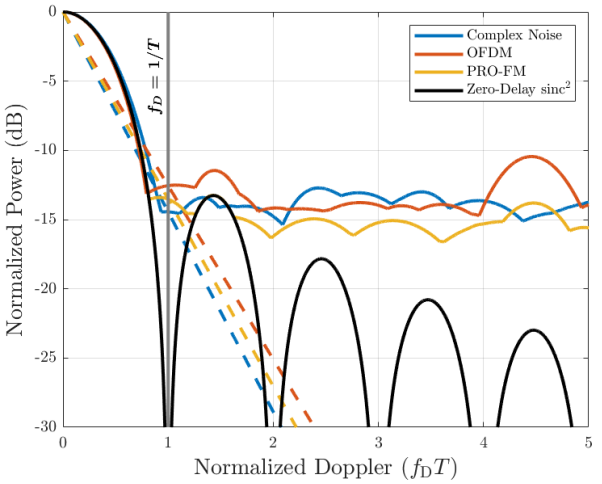

Fig. 4. Delay/Doppler ridge η (solid traces) via (2) and loss line approximation (dashed traces) via (3) and (4) for individual noise-like waveforms at TB = 100.

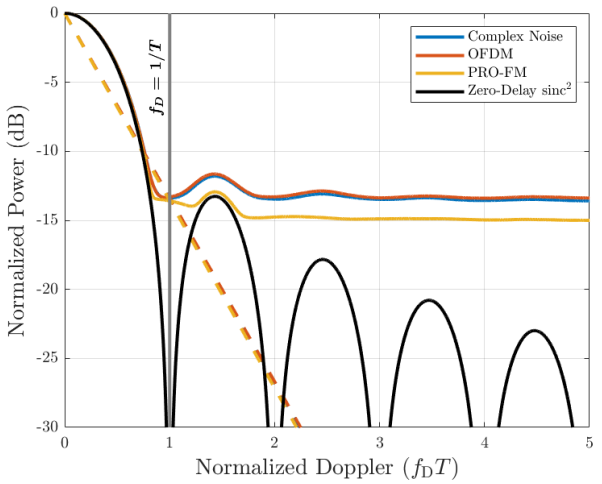

Fig. 5. Delay/Doppler ridge $\bar{\eta}$ (solid traces) via (7) and loss line approximation (dashed traces) via (8) and (9) for L = 1000 independent noise-like waveforms of each class at TB = 100.

As expected, Table III reveals that (8) follows the sinc^2 Doppler roll-off as observed in Figs. 4 and 5 since there is no delay/Doppler ridge. It is interesting to note, however, that at the evaluation point of $f_{\rm D} = 1/T$ (i.e. $\alpha = 1$) the determination of ψ_α is not masked by the sinc^2 aspect and therefore captures the true maxima "floor" (at about –13.5 dB for this TB), which is rather flat thereafter (Fig. 5) aside from the presence of the first Doppler sidelobe from the sinc^2 response.

TABLE III
COMPARISON OF $\bar{\psi}_\alpha$ FROM (8) AT DIFFERENT α VALUES FOR NOISE-LIKE WAVEFORMS AT TB=100

	ψ_α, $\alpha = 0.25$	ψ_α, $\alpha = 0.5$	ψ_α, $\alpha = 1.0$
Complex Noise	–0.90 dB	–3.81 dB	–13.41 dB
OFDM	–0.89 dB	–3.80 dB	–13.39 dB
PRO-FM	–0.91 dB	–3.88 dB	–13.56 dB

It is again illustrative to plot (3) and (8), for $\alpha = 1$, as a function of *TB* for these waveform types, as shown in Figs. 6 and 7, respectively. Where the chirped waveforms in Fig. 3 all asymptotically approach a fixed value as *TB* increases, here we observe a trend toward a linear reduction in the maxima "floor" at higher *TB*. For instance, Fig. 7 reveals about 8.25 dB reduction over the decade from 10^2 to 10^3 that is due to increased dimensionality alone (i.e. not averaging).

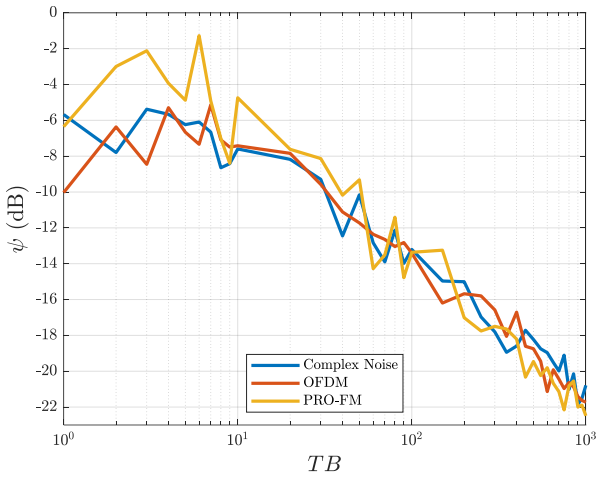

Fig. 6. Comparison of ψ from (3) for individual noise-like waveforms as a function of *TB* from 1 to 1000.

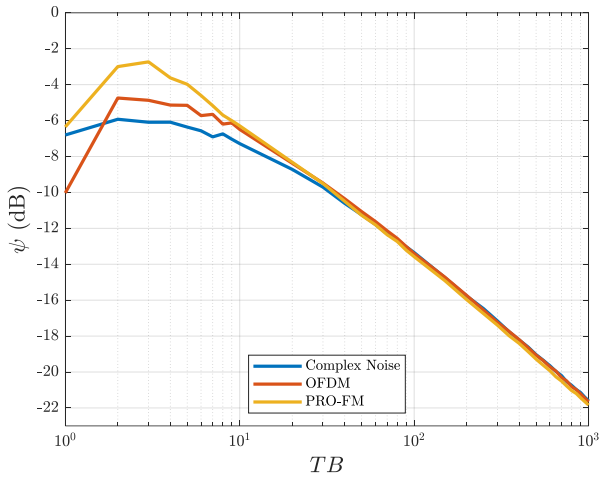

Fig. 7. Comparison of (8) for $\alpha = 1$ when averaging $L = 1000$ independent noise-like waveforms from each class as a function of *TB* from 1 to 1000.

An interesting variant of noise-like waveforms arises when combining with chirp waveforms, such as may be done to embed an information-bearing payload, which necessarily involves uncertainty [34-36]. Consider the PARC structure [35] in this context, which relies on the phase-attaching of communication and radar versions of continuous phase modulation (CPM). This digital implementation of FM can be expressed in the general form

$$s(t) = \exp\left\{ j\left(\theta_{\text{radar}}(t) + h\,\phi_{\text{comm}}(t) \right) \right\}. \qquad (10)$$

Here $\theta_{\text{radar}}(t)$ is the continuous phase function of time for the radar component while $\theta_{\text{comm}}(t)$ is the continuous communication function of time that can vary pulse-to-pulse according to the embedded information. The term *h* is the "modulation index" that scales the latter relative to the former, generally using small values << 1.

In this context, let $\theta_{\text{radar}}(t)$ correspond to the quadratic phase function of LFM so that $h = 0$ is a Doppler tolerant baseline. We allow $\theta_{\text{comm}}(t)$ to be a CPM implementation of a random bit stream as in [35], though the particular nature of this variable component is of less consequence than the scaling *h*. The impact of this component is shown in Fig. 8 when responses are averaged over $L = 1000$ independent waveforms for each case (individual instantiations are negligibly different).

Relative to the $h = 0$ (LFM) baseline, the incremental doubling from $h = 1/64$ up to $h = 1/8$ gradually realizes less Doppler tolerance. The loss line approximations likewise deviate more as *h* increases yet preserve the general trend in behavior, especially given the largely linear Doppler roll-off inscribed by the ridges.

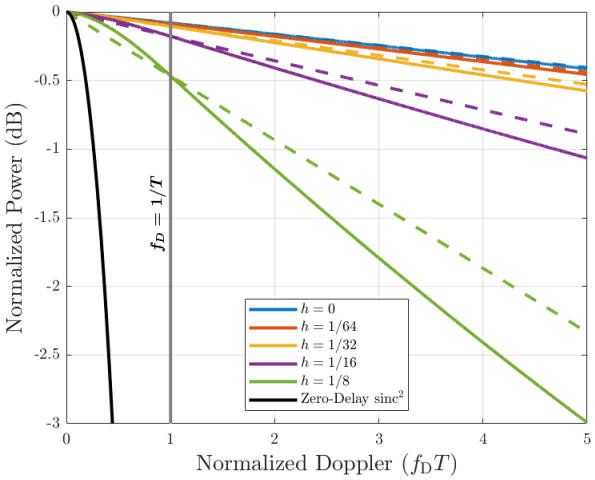

Fig. 8. Delay/Doppler ridge $\bar{\eta}$ (solid traces) via (7) and loss line approximation (dashed traces) via (8) and (9) for 1000 independent PARC waveforms for each value of *h* at *TB* = 100.

An additional take-away from Fig. 8 is the prospect of as-needed generation of new quasi-tolerant waveforms, which in principle could be produced according to some required degree of tolerance by simply phase-attaching a random continuous phase function (of arbitrary type) to LFM using a prescribed value of *h*. Fig. 9 illustrates the evaluation of (8) for $\alpha = 1$ averaged over $L = 1000$ waveforms as a function of *h* from 0 to 1/8, illustrating a clear trend that could be used to select a value of *h*.

Moreover, consider the evaluation of (8) for $\alpha = 1$ as a function of *TB* that is depicted in Fig. 10, where we observe a trend with increasing *TB* similar to that of LFM in Fig. 3. While the $h = 1/8$ case does exhibit more noticeable deviation, it is approaching an asymptote of only about –0.5 dB (instead of 0 dB) that is still quite reasonable from a Doppler tolerance perspective.

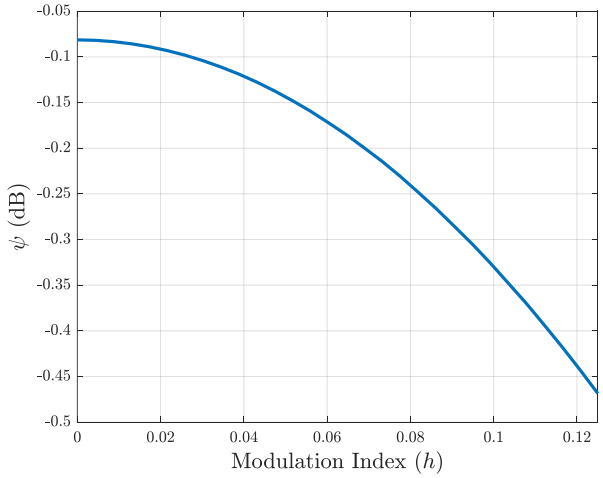

Fig. 9. Comparison of (8) for $\alpha = 1$ when averaging $L = 1000$ independent PARC waveforms for $TB = 100$ as a function of h.

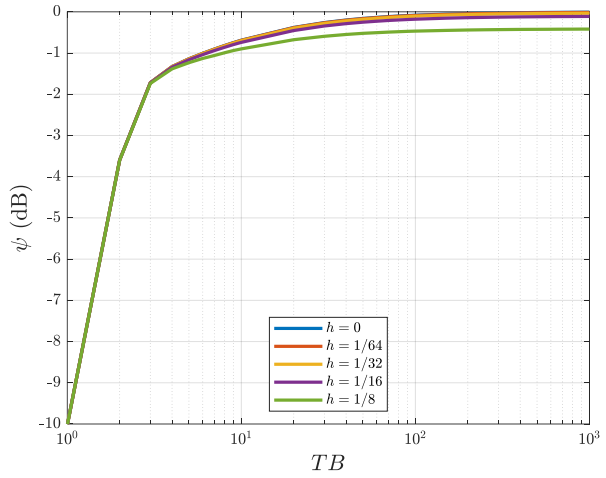

Fig. 10. Comparison of (8) for $\alpha = 1$ when averaging $L = 1000$ independent PARC waveforms for each value of h as a function of TB from 1 to 1000.

C. Phase Codes

There has been significant research interest in phase codes, both binary and polyphase, due to the significant design freedom they provide (see [12]). For phase-coded waveforms, code length is analogous to TB, which is convenient for comparison purposes.

Of course, an important consideration for phase codes is physical implementation since the abrupt transition between phase values introduces distortion [43] that may limit their utility. For binary codes this effect is generally handled by employing minimum shift keying (MSK) [44] or the binary-to-quadriphase (BTQ) transformation [45]. Here we use the former to examine Doppler tolerance of random binary codes.

Likewise, the polyphase-coded frequency modulation (PCFM) framework can be used to implement arbitrary polyphase codes [43]. Given the significant amount of theoretical work involving polyphase codes excluding this mapping, we shall examine Doppler tolerance of random polyphase codes both without and with the PCFM implementation, denoting the former as "direct".

For a code length of $N = 100 \approx TB$ and chip widths scaled to preserve 3-dB bandwidth across the different classes, Figs. 11 and 12 illustrate individual waveform instantiations and average responses, respectively. Because the codes are random, the resulting thumbtack responses realize Doppler metric values that are quite similar to those obtained for the random signals in Figs. 4 and 5. Likewise, the sinc^2 mainlobe roll-off again dominates until the "floor" becomes visible at $f_D = 1/T$.

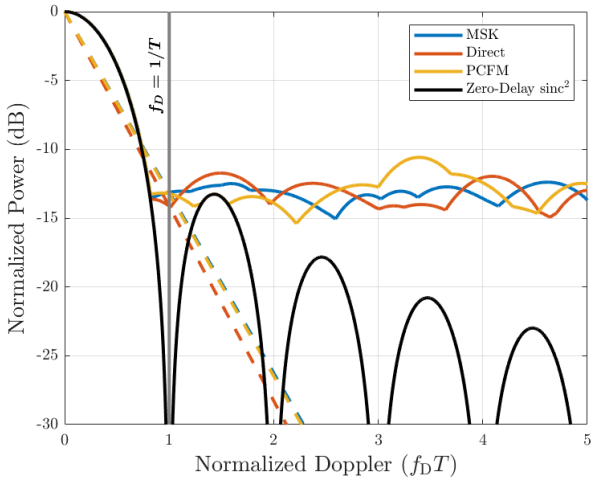

Fig. 11. Delay/Doppler ridge η (solid traces) via (2) and line approximation (dashed traces) via (3) and (4) for individual phase-coded waveforms at $N = 100$.

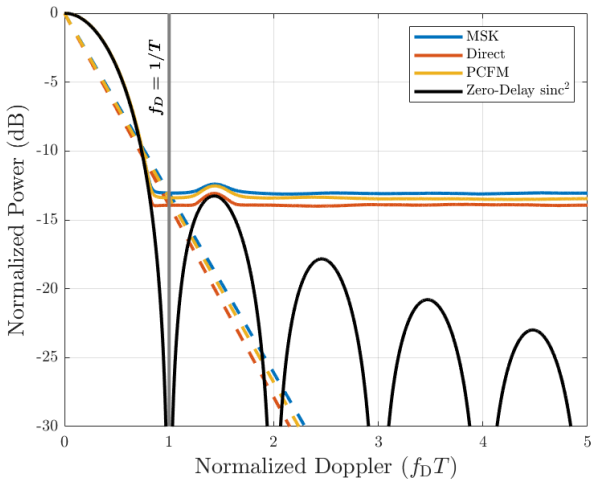

Fig. 12. Delay/Doppler ridge $\bar{\eta}$ (solid traces) via (7) and loss line approximation (dashed traces) via (8) and (9) for $L = 1000$ independent phase-coded waveforms of each class at $N = 100$.

Like Fig. 7 that plotted the averaged Doppler metric over $L = 1000$ independent waveforms from each class as a function of TB, Fig. 13 does so for each class of phase-coded waveform as a function of $N \approx TB$. We observe a similar almost-linear trend of 8 dB reduction over the decade from 10^2 to 10^3 due to increased dimensionality alone. One important take-away is that for $N > 10$ the direct code representation that contains abrupt phase-changes yields a Doppler tolerance metric only 0.5 to 1 dB less than the MSK and PCFM implemented versions, which are physically realizable.

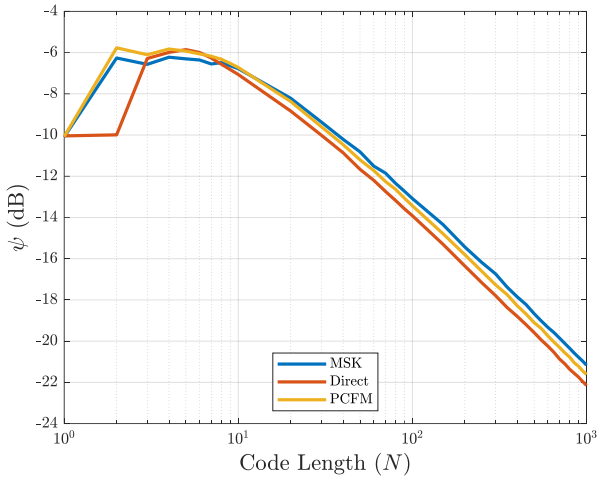

Fig. 13. Comparison of (8) for $\alpha = 1$ when averaging $L = 1000$ independent phase-coded waveforms from each class as a function of N from 1 to 1000.

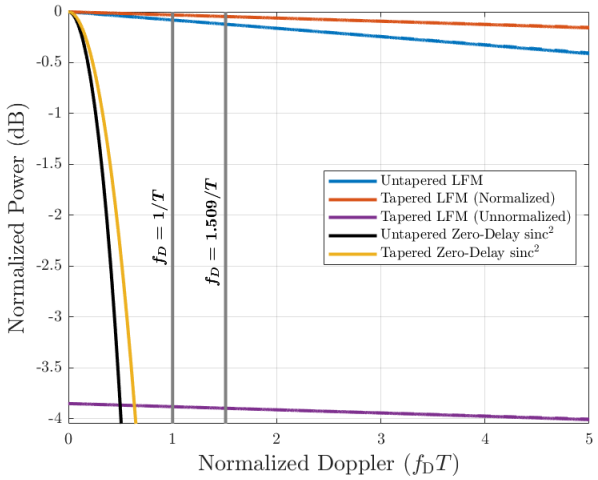

Fig. 14. Delay/Doppler ridge η (solid traces) via (2) and loss line approximation (dashed traces) via (3) and (6) for LFM and Taylor tapered LFM at $TB = 100$. The original and tapered zero-Doppler responses are the black and yellow traces while the labeled gray lines denote where respective first-nulls are evaluated.

IV. Tapering

As noted in the lead-up to (6), an interesting extension of this Doppler tolerance metric involves the inclusion of tapering, which then enables a before/after comparison. Of particular relevance is the fact that the first Doppler null shifts outward as a result of the broader mainlobe caused by tapering. Because doing so also de-emphasizes the frequencies at the edges of the band for chirped waveforms, the ensuing reduced bandwidth caused by spectral shaping is likewise the reason for degraded range resolution (i.e. same root cause, but different effects).

Noting the compressed vertical axis relative to Fig. 2, Fig. 14 illustrates the ridge and associated loss line approximations for LFM (dark blue) and for when the received (now mismatched) filter is Taylor tapered (red), with the latter peak-normalized by the tapered version of $A(0,0)$. The dashed lines are nearly indistinguishable from the solid traces of the ridges for all cases. In this normalized perspective we find that tapering actually improves Doppler tolerance. The alternative implementation involving the square-root of the taper on both waveform and filter yields identical results.

While the resulting ψ values of −0.0808 dB and −0.0464 dB for LFM and tapered LFM are also different, these alone are insufficient to make a comparison because they respectively correspond to different Doppler evaluation points of $f_D = 1/T$ and $f_D = 1.509/T$ due to the change in first Doppler null. However, because the loss line approximation is so close to the ridge in both cases, it is easy to extrapolate their behavior at a common Doppler reference.

Doppler tolerance alone – meaning the amount of deviation from $A(0,0)$ – is not sufficient in this context. The purple traces (indistinguishable solid and dashed) in Fig. 14 remove this normalization so that the 3.85 dB loss is included. If tapering loss is acceptable, which it is for some applications, then a modest improvement in Doppler tolerance is obtained.

It is also useful to evaluate ψ as a function of TB without and with tapering (still receive-only) as depicted in Fig. 15. While both cases asymptotically approach 0 dB (noting that the tapered case is once again normalized), at values of $TB > 5$ the tapered tolerance is better, though the distinction greatly diminishes at higher TB.

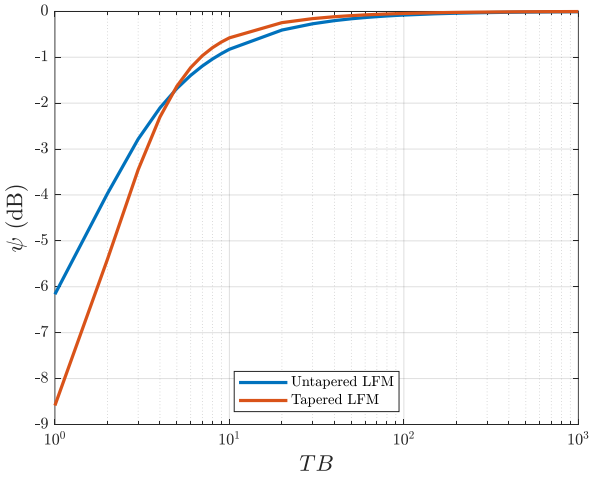

Fig. 15. Comparison of ψ from (3) for LFM without and with Taylor tapering as a function of TB from 1 to 1000.

V. Wideband Doppler Tolerance Metric

Finally, a wideband version of the Doppler tolerance metric in (2) and (3) can be readily obtained by converting Doppler frequency into radial velocity v as

$$v = c\left(\frac{f_D}{2f_c}\right), \tag{11}$$

with f_c the carrier frequency and c the speed of light. Using the well-known definition of percent (or fractional) bandwidth

$$\%B = \frac{B}{f_c}, \tag{12}$$

we can rearrange (12) and substitute into (11) to yield

$$v = 0.5c\left(\frac{\%B\, f_D}{B}\right). \tag{13}$$

The delay/Doppler ridge is then extracted from the (magnitude squared) wideband ambiguity function [5]

$$A_{WB}(\tau, v) = \left| \int_{-\infty}^{\infty} s\left(\left(\tfrac{c+v}{c-v}\right)t\right)\, s^*(t+\tau)\, e^{j4\pi v f_c t/c}\, dt \right|^2 \tag{14}$$

by posing (2) as

$$\eta_{WB}(v) = \frac{\max_{\tau} A_{WB}(\tau, v)}{A_{WB}(0,0)}. \tag{15}$$

The wideband version of metric (3) is subsequently obtained from (15) when (13) is evaluated at the corresponding (first Doppler null) velocity of

$$\begin{aligned} v_{null} = c\left(\frac{\%B\, f_D}{2B}\right)\Bigg|_{f_D = 1/T} &= 0.5c\left(\frac{\%B}{TB}\right) \\ &= 0.5c\left(\frac{1}{f_c T}\right), \end{aligned} \tag{16}$$

thereby yielding

$$\psi_{WB} = 10\log_{10}\left(\eta_{WB}(v = v_{null})\right)\ \text{dB}, \tag{17}$$

where the second line of (16) is an alternative perspective obtained by substituting in (12). Consequently, the loss line approximation of (4) becomes

$$\text{loss}(v) \approx \left(\frac{\psi_{WB}}{v_{null}}\right)|v|\ \text{dB}. \tag{18}$$

Setting $v_{null} \to \alpha\beta v_{null}$ likewise incorporates (5) and (6).

For example, Fig. 16 compares HFM (top) and LFM (bottom) as a function of TB when percent bandwidth is 25%. While the traces appear to be similar, note the significant difference in values along the vertical axes, illustrating far superior Doppler tolerance (some say "invariance") for hyperbolic FM. Due to the alternative perspective in (16), varying $\%B$ for a fixed TB would effectively yield the same relationship given a constant value of T.

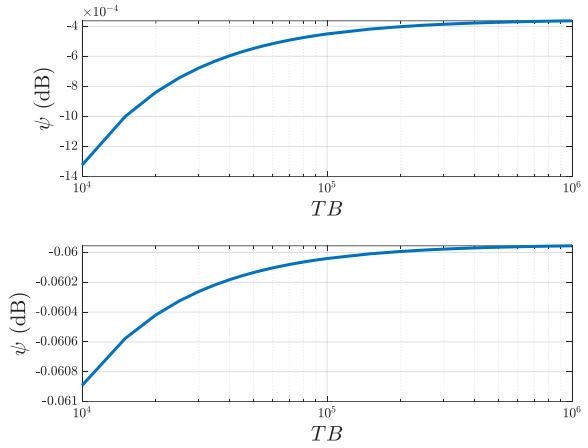

Fig. 16. Comparison of ψ_{WB} from (17) for HFM (top) and LFM (bottom) as a function of TB from 10^4 to 10^6 for $\%B$ = 25%.

VI. Conclusions

A recently-proposed, simple metric for Doppler tolerance has been further developed and evaluated for a variety of different waveform classes. This metric introduces a loss line approximation that itself can be used to infer properties of waveforms. It has been found that degrees of quasi-tolerance can be achieved when a chirp-like structure is preserved, thereby permitting tolerance to become part of the overall waveform design trade-space. This metric has likewise been extended for use with tapering and in a wideband context.

References

[1] Woodward, P.M., *Probability and Information Theory, with Applications to Radar*, Pergamon Press, New York, NY, 1953.

[2] Rihaczek, A., *Principles of High-Resolution Radar*, Artech House, Boston, MA, 1969.

[3] Rihaczek, A.W., "Delay-Doppler ambiguity function for wideband signals," *IEEE Trans. Aerospace & Electronic Systems*, vol. AES-3, no. 4, pp. 705-711, July 1967.

[4] Sibul L., Ziomek, L., "Generalized wideband crossambiguity function," *IEEE Intl. Conf. Acoustics, Speech, & Signal Processing*, Atlanta, GA, Mar./Apr. 1981, pp. 1239-1242.

[5] Altes, R.A., "Some invariance properties of the wide-band ambiguity function," *Journal of the Acoustical Society of America*, vol. 53, no. 4, pp. 1154-1160, Apr. 1973.

[6] Kelly, E.J., Wishner, R.P., "Matched-filter theory for high-velocity accelerating targets," *IEEE Trans. Military Electronics*, vol. 9, no. 1, pp. 56-69, Jan. 1965.

[7] Rihaczek, A.W., "Radar resolution of moving targets," *IEEE Trans. Information Theory*, vol. IT-13, no. 1, pp. 51-56, Jan. 1967.

[8] Hines, P.C., Murphy, S.M., Bates, J.R., Coffin, M., "Ambiguity functions, wideband and narrowband approximations, and high duty cycle sonars," *Underwater Acoustics Conf.*, Skiathos, Greece, Sept. 2017.

[9] Franken, G.E.A., Nikookar, H., van Genderen, P., "Doppler tolerance of OFDM-coded radar signals," *European Radar Conference*, Manchester, UK, Sept. 2006, pp. 108-111.

[10] Setlur, P., Hollon, J., Arasu K.T., Rangaswamy, M., "On a formal measure of Doppler tolerance," *IEEE Radar Conf.*, Seattle, WA, May 2017, pp. 1751-1756.

[11] Correll, B., Butler, T.D., Swanson, C.N., Narayanan, R.M., "A formal study of the Doppler tolerance of Costas and Sudoku waveforms," *IEEE Radar Conf.*, Atlanta, GA, May 2021.

[12] Blunt, S.D., Mokole, E.L., "Overview of radar waveform diversity," *IEEE Aerospace & Electronic Systems Mag.*, vol. 31, no. 11, pp. 2-42, Nov. 2016.

[13] Rihaczek, A.W., "Doppler-tolerant signal waveforms," *Proc. IEEE*, vol. 54, no. 6, pp. 849-857, June 1966.

[14] Balleri, A., Farina, A., "Ambiguity function and accuracy of the hyperbolic chirp: comparison with the linear chirp," *IET Radar, Sonar & Navigation*, vol. 11, no. 1, pp. 142-153, Jan. 2017.

[15] McCargar, R.K., Jones, J.J., Smith G.E., Garry, J.L., "Experimental demonstration of a highly Doppler-tolerant pulsed waveform," *IEEE Trans. Aerospace & Electronic Systems*, vol. 57, no. 6, pp. 4188-4196, Dec. 2021.

[16] Johnson, R.A., Titlebaum, E.L., "Range-Doppler uncoupling in the Doppler tolerant bat signal," *IEEE Ultrasonics Symp.*, Boston, MA, Oct. 1972, pp. 64-67.

[17] Griffiths, H., Baker, C., "The signal and interference environment in passive bistatic radar," *Information, Decision & Control Conf.*, Adelaide, Australia, Feb. 2007.

[18] Palmer, J.E., Harms, H.A., Searle S.J., Davis, L., "DVB-T passive radar signal processing," *IEEE Trans. Signal Processing*, vol. 61, no. 8, pp. 2116-2126, Apr. 2013.

[19] Colone, F., Woodbridge, K., Guo, H., Mason, D., Baker, C.J., "Ambiguity function analysis of wireless LAN transmissions for passive radar," *IEEE Trans. Aerospace & Electronic Systems*, vol. 47, no. 1, pp. 240-264, Jan. 2011.

[20] Stein, S., "Algorithms for ambiguity function processing," *IEEE Trans. Acoustics, Speech, & Signal Processing*, vol. 29, no. 3, pp. 588-599, June 1981.

[21] Ilioudis, C.V., Clemente, C., Proudler, I.K., Soraghan, J., "Generalized ambiguity function for MIMO radar systems," *IEEE Trans. Aerospace & Electronic Systems*, vol. 55, no. 6, pp. 2629-2646, Dec. 2019.

[22] San Antonio, G., Fuhrmann, D.R., Robey, F.C., "MIMO radar ambiguity functions," *IEEE Journal Selected Topics in Signal Processing*, vol. 1, no. 1, pp. 167-177, June 2007.

[23] Gogineni, S., Rangaswamy, M., Rigling, B.D., Nehorai, A., "Ambiguity function analysis for UMTS-based passive multistatic radar," *IEEE Trans. Signal Processing*, vol. 62, no. 11, pp. 2945-2957, June 2014.

[24] Horton, B.M., "Noise-modulated distance measuring systems," *Proc. IRE*, vol. 47, no. 5, pp. 821-828, May 1959.

[25] Malanowski, M., Kulpa, K., Baczyk, M., Maslikowski, L., "Noise vs. deterministic waveform radar – possibilities and limitations," *IEEE Aerospace & Systems Mag*., vol. 35, no. 10, pp. 8-19, Oct. 2020.

[26] Costas, J.P., "A study of a class of detection waveforms having nearly ideal range-Doppler ambiguity properties," *Proc. IEEE*, vol. 72, no. 8, pp. 996-1009, Aug. 1984.

[27] Donohoe, J.P., Ingels, F.M., "The ambiguity properties of FSK/PSK signals," *IEEE Intl. Conf. on Radar*, Arlington, VA, May 1990, pp. 268-273.

[28] Farnane, K., Minaoui, K., Rouijel, A., Aboutajdine, D., "Analysis of the ambiguity function for phase-coded waveforms," *IEEE/ACS Intl. Conf. Computer Systems & Applications*, Marrakech, Morocco, Nov. 2015.

[29] Whiteley, T.B., Adrian, D.J., "Random FM autocorrelation fuze system," U.S. Patent #4,220,952, issued Sept. 2, 1980, application filed Feb. 17, 1956.

[30] Axelsson, S.R.J., "Noise radar using random phase and frequency modulation*" IEEE Trans. Geoscience & Remote Sensing*, vol. 42, no. 11, pp. 2370–2384, Nov. 2004.

[31] Pralon, L., Pompeo, B., Fortes, J.M., "Stochastic analysis of random frequency modulated waveforms for noise radar systems," *IEEE Trans. Aerospace & Electronic Systems*, vol. 51, no. 2, pp. 1447-1461, Apr. 2015.

[32] Blunt, S.D., *et al*., "Principles and applications of random FM radar waveform design," *IEEE Aerospace & Electronic Systems Mag.*, vol. 35, no. 10, pp. 20-28, Oct. 2020.

[33] Pralon, L., Beltrao, G., Pompeo, B., Pralon M., Fortes, J.M., "Near-thumbtack ambiguity function of random frequency modulated signals," *IEEE Radar Conf.*, Seattle, WA, May 2017, pp. 0352-0355.

[34] Chen, X., Wang, X., Xu, S., Zhang, J., "A novel radar waveform compatible with communication," *Intl. Conf. Computational Problem-Solving*, pp. 177–181, Oct. 2011.

[35] Sahin, C., Jakabosky, J., McCormick, P.M., Metcalf, J.G., Blunt, S.D., "A novel approach for embedding communication symbols into physical radar waveforms," *IEEE Radar Conf.*, Seattle, WA, May 2017, pp. 1498-1503.

[36] Zhang, Z., Qu, Y., Wu, Z., Nowak, M.J., Ellinger, J., Wicks, M.C., "RF steganography via LFM chirp radar signals," IEEE Trans. Aerospace & Electronic Systems, vol. 54, no. 3, pp. 1221-1236, June 2018.

[37] Stralka, J.P., Thomas, D.D., "Practical waveform diversity applications and implementation challenges," *IEEE Radar Conf.*, Atlanta, GA, May 2021.

[38] Mohr, C.A., McCormick, P.M., Topliff, C.A., Blunt, S.D., Baden, J.M., "Gradient-based optimization of PCFM radar waveforms," *IEEE Trans. Aerospace & Electronic Systems*, vol. 57, no. 2, pp. 935-956, Apr. 2021.

[39] Collins, T., Atkins, P., "Nonlinear frequency modulation chirps for active sonar," *IEE Proc. Radar, Sonar & Navigation*, vol. 146, no. 6, pp. 312-316, Dec. 1999.

[40] Yue, W., Zhang, Y., "A novel nonlinear frequency modulation waveform design aimed at side-lobe reduction," *IEEE Intl. Conf. Signal Processing, Communications & Computing*, Guilin, China, Aug. 2014, pp.613-618.

[41] Gao, C., The, K.C., Liu, A., "Frequency diversity waveform with NLFM signals," *Intl. Conf. Information, Communications & Signal Processing*, Singapore, Dec. 2015.

[42] Jakabosky, J., Blunt, S.D., Himed, B., "Spectral-shape optimized FM noise radar for pulse agility," *IEEE Radar Conf.*, Philadelphia, PA, May 2016.

[43] Blunt, S.D., Cook, M., Jakabosky, J., De Graaf, J., Perrins, E., "Polyphase-coded FM (PCFM) radar waveforms, part I: implementation," *IEEE Trans. Aerospace & Electronic Systems*, vol. 50, no. 3, pp. 2218-2229, July 2014.

[44] Faust, H.H., Connolly, B., Firestone, T.M., Chen, R.C., Cantrell, B.H., Mokole, E.L., "A spectrally clean transmitting system for solid-state phased-array radars," *IEEE Radar Conf., Philadelphia, PA, Apr.* 2004, pp. 140-144.

[45] Taylor, J.W., Blinchikoff, H.J., "Quadriphase code – a radar pulse compression signal with unique characteristics," *IEEE Trans. Aerospace & Electronic Systems*, vol. 24, no. 2, pp. 156-170, May 1988.

[46] Levanon, N., "The periodic ambiguity function — Its validity and value," *IEEE Radar Conf.*, Arlington, VA, May 2010, pp. 204-208.